JACS
JOURNAL OF THE AMERICAN CHEMICAL SOCIETY
pubs.acs.org/JACS
Article

Photochemical H_2 Evolution from Bis(diphosphine)nickel Hydrides Enables Low-Overpotential Electrocatalysis

Bethany M. Stratakes, Kaylee A. Wells, Daniel A. Kurtz, Felix N. Castellano, and Alexander J. M. Miller*

Cite This: https://doi.org/10.1021/jacs.1c10628
Read Online
ACCESS | Metrics & More | Article Recommendations | Supporting Information

ABSTRACT: Molecules capable of both harvesting light and forming new chemical bonds hold promise for applications in the generation of solar fuels, but such first-row transition metal photoelectrocatalysts are lacking. Here we report nickel photoelectrocatalysts for H_2 evolution, leveraging visible-light-driven photochemical H_2 evolution from bis(diphosphine)nickel hydride complexes. A suite of experimental and theoretical analyses, including time-resolved spectroscopy and continuous irradiation quantum yield measurements, led to a proposed mechanism of H_2 evolution involving a short-lived singlet excited state that undergoes homolysis of the Ni−H bond. Thermodynamic analyses provide a basis for understanding and predicting the observed photoelectrocatalytic H_2 evolution by a 3d transition metal based catalyst. Of particular note is the dramatic change in the electrochemical overpotential: in the dark, the nickel complexes require strong acids and therefore high overpotentials for electrocatalysis; but under illumination, the use of weaker acids at the same applied potential results in a more than 500 mV improvement in electrochemical overpotential. New insight into first-row transition metal hydride photochemistry thus enables photoelectrocatalytic H_2 evolution without electrochemical overpotential (at the thermodynamic potential or 0 mV overpotential). This catalyst system does not require sacrificial chemical reductants or light-harvesting semiconductor materials and produces H_2 at rates similar to molecular catalysts attached to silicon.

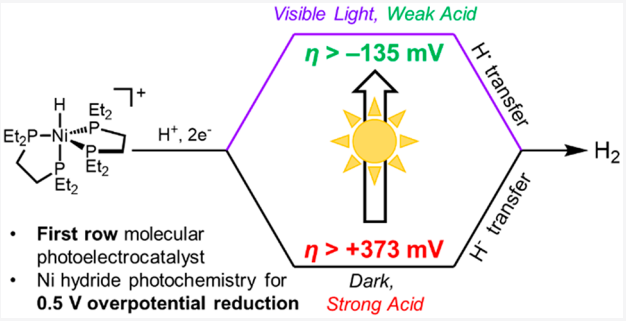

INTRODUCTION

An emerging approach in the synthesis of solar fuels utilizes molecular photoelectrocatalysts capable of both photochemical H_2 evolution and electrochemical regeneration.[1] Combining multiple functions (such as photosensitization, catalysis, and regeneration) into one transition metal complex could enhance efficiency. We introduced this concept in 2014, demonstrating that $[Cp^*Ir(bpy)H]^+$ and analogues first reported by Ziessel[2−7] catalyze sustained H_2 evolution from neutral water with ca. 10% external quantum efficiency and >95% Faradaic efficiency when simultaneously illuminated with visible light and biased at a low electrochemical overpotential.[8] In acetonitrile solution, the same family of catalysts can even achieve *negative* overpotentials under visible light illumination.[9] Additional single-component photoelectrocatalysts for H_2 evolution based on Ru and Rh have appeared recently, but like the Ir systems these also rely on precious metals (Figure 1).[10−12] It is likely that any practical system for solar fuels generation will require the light harvester to be composed of abundant and affordable elements, but to date, there have been no reports of molecular photoelectrocatalysts based on first-row transition metal complexes.

A major limitation in developing photoelectrocatalysts based on abundant elements is the lack of well-defined photochemistry of 3d transition metal hydride complexes. Many

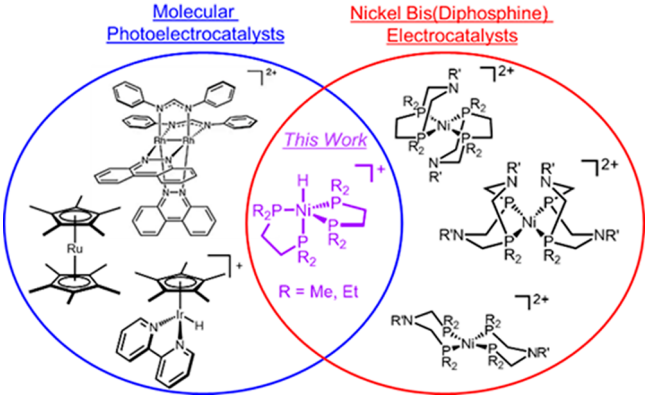

Figure 1. Examples of molecular photoelectrocatalysts[8−12] (left, blue) and nickel bis(diphosphine) electrocatalysts[13,14] (right, red) for H_2 evolution. This work (center, purple) represents the first example of a first-row transition metal complex operating as a molecular photoelectrocatalyst.

Received: October 9, 2021

first-row transition meal complexes have accessible ligand field states that are associated with rapid nonradiative decay or unproductive ligand dissociation reactions.[15] For example, reviews note that $[Cr_2(\mu\text{-H})(CO)_{10}]^-$, $CpCr(CO)_3H$, $Mn(CO)_5H$, $HCo(CO)_4$, and $Fe(H)_2(N_2)(PEtPh_2)_2$ undergo photochemical dissociation of CO or N_2 rather than productive H_2 evolution.[16,17] A noteworthy exception is the diiron complex $[Fe_2(CO)_4(\mu\text{-}Ph_2PCH{=}CHPPh_2)(\mu\text{-propanedithiolate})(\mu\text{-H})]^+$, which also predominantly releases CO upon photoexcitation but does offer a low-quantum-yield pathway for H_2 evolution that was leveraged for "sensitizer-free" photocatalysis.[18−20] This photochemical reaction requires stoichiometric sacrificial chemical reductants, leading to large amounts of waste byproducts. Ni dithiolene complexes also exhibit sensitizer-free H_2 evolution catalysis driven by sacrificial reductants, although no nickel hydride was observed or invoked in that work.[21] More recently, a pincer-ligated nickel(II) hydride was found to undergo photochemical H_2 evolution with UV light (>305 nm).[22] Recent examples of photochemical halogen atom release, C−O reductive elimination, and Ni−C homolysis to produce a free aryl radical provided further evidence that nickel may be a promising element for photoelectrochemical H_2 evolution.[23−25]

While reports of photochemical H_2 evolution from nickel hydride complexes are scarce,[26] hydridonickel complexes are key intermediates in dark electrochemical H_2 evolution catalysis. The iconic class of nickel catalysts bearing two diphosphines containing one or more amine functional groups serve as a prime example (Figure 1), with rates of electrocatalysis exceeding 1600000 s^{-1} and overpotentials required to reach half the maximum turnover frequency (TOF) ranging from +260 to +1200 mV.[27,28] Prior efforts to drive these reactions using solar energy have taken multicomponent approaches that physically and temporally separate the light absorption and bond formation events. Homogeneous approaches pair leading Ni electrocatalysts with separate photosensitizers, with regeneration occurring via sacrificial chemical reductants.[29] Inherent limitations in photon flux, coupled with challenges related to catalyst and photosensitizer durability, have limited the catalytic turnover frequencies of light-driven H_2 evolution to range from 0.0056 to 0.13 s^{-1}.[30,31] Heterogeneous approaches in which variants of these Ni catalysts are attached to the surface of a semiconductor light-absorbing material have also been pursued,[32−35] with a leading example reporting photoelectrocatalytic H_2 evolution at $\eta = 0$ V (no overpotential required) and TOF = 0.007 s^{-1}.[35]

We hypothesized that an appropriate nickel(II) hydride complex could function as a single-component photoelectrocatalyst through a photoinduced H_2 evolution step. This could lead to more efficient light-driven fuel generation and would provide fundamental insight into metal hydride photochemistry. Choosing to avoid complexes with pendent amines that could unproductively quench excited states, we were drawn to simple nickel bis(diphosphine) complexes with rich structural diversity and wide knowledge of thermodynamic parameters (acidity, hydricity, and reduction potentials).[36] Early studies of nickel bis(diphosphine) complexes focused on H_2 oxidation.[37,38] A few examples of H_2 evolution have been reported, requiring strong acids and operating at overpotentials of ca. 500 mV.[39,40] High overpotentials are often incurred with molecular electrocatalysts because the thermodynamic potential for H^+ reduction to H_2 shifts to positive potential with increasingly acidic media while the catalytic onset remains at the same potential for most catalysts. The use of weak acids thus constitutes a general approach to lowering overpotential. However, nickel bis(diphosphine) hydride complexes are incapable of producing H_2 with weak acids under normal (dark) electrochemical conditions. We hypothesized that *photochemical* H_2 evolution could proceed with weak acids, thereby enabling electrocatalysis with dramatically reduced overpotential by integrating light absorption and catalysis in a single system.[41]

Herein, we report quantitative visible-light-driven H_2 evolution from the well-defined nickel hydrides $[HNi(dmpe)_2]^+$ (dmpe = 1,2-bis(dimethylphosphino)ethane) and $[HNi(depe)_2]^+$ (depe = 1,2-bis(diethylphosphino)ethane). Time-resolved spectroscopy and steady-state photolysis studies implicate excited-state Ni−H bond homolysis as the key step leading to both H_2 evolution or hydrogen atom transfer (HAT) reactivity. The photochemical H_2 evolution is paired with electrochemical generation of the hydrides to demonstrate the first example of molecular photoelectrochemical H_2 evolution from a first-row transition metal complex. The single-component photoelectrocatalysts operate with acids that are much weaker than required for dark electrocatalysis, leading to a dramatic 500 mV reduction in overpotential as well as operation at the thermodynamic potential (0 V overpotential).

RESULTS AND DISCUSSION

Initial Observation of Photochemical H_2 Evolution from Ni−H Complexes. The evaluation of the photochemical reactivity of $[HNi(dmpe)_2][PF_6]$ ($\mathbf{1H^+}$) and $[HNi(depe)_2][PF_6]$ ($\mathbf{2H^+}$) was initially pursued after noticing that samples of the hydrides would degrade in MeCN solutions exposed to ambient light. When protected from light, however, samples of $\mathbf{1H^+}$ and $\mathbf{2H^+}$ in MeCN remained stable for several days, with no reaction observed by NMR spectroscopy. Based on this observation, a more rigorous series of photolysis reactions was then pursued.

The bis(diphosphine)nickel hydride complexes were prepared as previously reported by DuBois and co-workers.[36,42] The solid-state structure of the $S = 0$ five-coordinate nickel(II) complex $\mathbf{2H^+}$ is presented for the first time in Figure 2, enabled

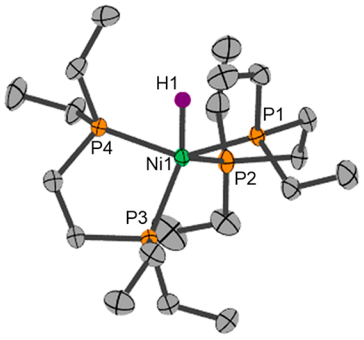

Figure 2. Structural representation of $\mathbf{2H^+}$ with ellipsoids drawn at the 50% probability level. All hydrogen atoms (except for the hydride) and the PF_6^- counterion are omitted for clarity. Selected bond distances (Å) and angles (deg): Ni1−H1 1.41(4), Ni1−P1 2.2091(6), Ni1−P2 2.1685(5), Ni1−P3 2.1683(6), Ni1−P4 2.2197(7), P1−Ni1−P2 90.25(2), P1−Ni1−P3 113.38(2), P1−Ni1−P4 110.02(2), P2−Ni1−P3 139.21(2), P2−Ni1−P4 114.12(2), and P3−Ni1−P4 89.41(2).

https://doi.org/10.1021/jacs.1c10628
J. Am. Chem. Soc. XXXX, XXX, XXX−XXX

by growth of single crystals from vapor diffusion of Et_2O into a MeCN solution of $\mathbf{2H}^+$ at −30 °C. An approximately trigonal-bipyramidal geometry is observed in the solid state, with distinct axial and equatorial phosphorus donors. In solution, however, all four phosphorus donors are equivalent by NMR spectroscopy; this has been attributed either to fluxional exchange of the axial and equatorial phosphorus donors or to adoption of a square-pyramidal solution structure.[42] Nickel complexes that could form during H_2 evolution were also accessed by literature routes, providing the S = 0 nickel(II) complexes $[L_2Ni]^{2+}$ (L = dmpe or depe), which forms a five-coordinate complex with the solvent in MeCN solutions, and the tetrahedral d^{10} nickel(0) complexes L_2Ni (L = dmpe or depe).

Illumination of 2.5 μmol of dmpe complex $\mathbf{1H}^+$ in 500 μL of CD_3CN (5 mM Ni) with 405 nm light for 3.5 h resulted in clean conversion to the dicationic nickel(II) complex $[Ni(dmpe)_2(MeCN)][PF_6]_2$ ($\mathbf{1}^{2+}$, 1.25 μmol) and the neutral, partially insoluble nickel(0) complex $Ni(dmpe)_2$ ($\mathbf{1}°$, 1.19 μmol) according to ^1H and $^{31}P\{^1H\}$ NMR spectroscopy (Scheme 1).[36] H_2 was not observed by ^1H NMR spectroscopy

Scheme 1. Photochemical Reactivity of $\mathbf{1H}^+$ and $\mathbf{2H}^+$ in MeCN in the Absence of Acid under 405 nm Illumination

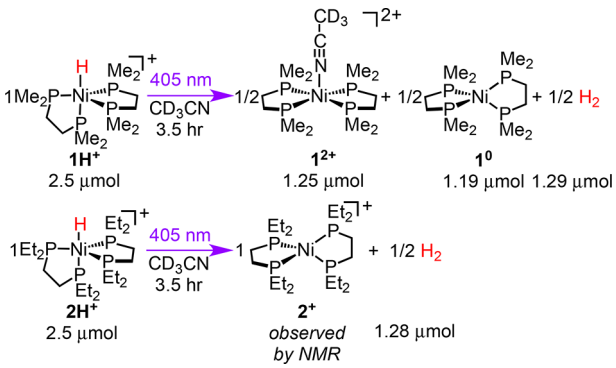

due to loss to headspace; however, it was produced in 1.29 ± 0.12 μmol yield (maximum theoretical yield: 1.25 μmol) as quantified by headspace gas chromatography (GC) analysis. The data are consistent with a stoichiometry of 1 equiv of Ni hydride producing 1/2 equiv of H_2, which would correspond to a maximum theoretical yield of 1.25 μmol of H_2 (103 ± 5% yield). Table S3 summarizes all of the NMR-scale photochemical H_2 evolution data. Control reactions monitoring solutions of $\mathbf{1H}^+$ in the dark showed no conversion by NMR spectroscopy, and no H_2 was detected by GC.

The depe complex $\mathbf{2H}^+$ (2.5 μmol) also reacts upon illumination of 5 mM CD_3CN solutions with 405 nm light for 3.5 h (Scheme 1), generating 1.28 μmol (102 ± 5% yield) of H_2 gas by GC (again, there was no conversion in the dark, at room temperature or at 40 °C). Photolysis of $\mathbf{2H}^+$ produced only trace amounts of the dicationic complex $[Ni(depe)_2][PF_6]_2$, $\mathbf{2}^{2+}$, by ^1H NMR spectroscopy, with broad resonances instead pointing to the formation of a paramagnetic nickel(I) complex, $[Ni(depe)_2][PF_6]$, $\mathbf{2}^+$, as the dominant product. A preparative scale photolysis produced 99% yield of paramagnetic $\mathbf{2}^+$ in ∼90% purity. Elemental analysis of the product was consistent with a nickel(I) complex of formula $[Ni(depe)_2][PF_6]$ ($\mathbf{2}^+$). Magnetic susceptibility measurements on a solution containing $\mathbf{2}^+$ using the Evans's method gave μ_{eff} = 1.68 μ_B, corresponding nicely to an S = 1/2 state.

While nickel(I) bis(diphosphine) complexes are rarely isolated,[43] the distinct products formed upon photolysis of $\mathbf{1H}^+$ and $\mathbf{2H}^+$ are consistent with electrochemical studies. Prior cyclic voltammetry (CV) studies of $\mathbf{2}^{2+}$ exhibited two distinct 1e$^-$ reductions, suggesting that the nickel(I) species formed upon a single reduction is thermodynamically stable; in contrast, CV of $\mathbf{1}^{2+}$ reveals a single 2e$^-$ reduction, indicating that $[Ni(dmpe)_2][PF_6]$ ($\mathbf{1}^+$) is unstable with respect to disproportionation to $\mathbf{1}^{2+}$ and $\mathbf{1}°$.[36] The stability of $\mathbf{2}^+$ with respect to disproportionation into $\mathbf{2}^{2+}$ and $\mathbf{2}°$ can be estimated based on the difference in the $Ni^{II/I}$ and $Ni^{I/0}$ reduction potentials.[36] The 130 mV separation between these waves suggests that $\mathbf{2}^+$ will generate small equilibrium amounts of approximately $\mathbf{2}^{2+}$ and $\mathbf{2}°$ under the typical concentrations employed here (ca. 6% $\mathbf{2}^{2+}$ at 5 mM starting concentration of $\mathbf{2}^+$; see section II of the Supporting Information for details), in line with the observation of trace $\mathbf{2}^{2+}$ after photolysis of $\mathbf{2H}^+$. The lack of observed $\mathbf{2}°$ is attributed to electron transfer self-exchange between $\mathbf{2}^+$ and $\mathbf{2}°$ on the NMR time scale (even after addition of excess $\mathbf{2}°$ only a very broad ^{31}P NMR feature was observed, Figure S3).

The free energy for thermal (dark) H_2 evolution from $\mathbf{1H}^+$ and $\mathbf{2H}^+$ can be calculated on the basis of available thermodynamic data pertaining to the Ni−H bond dissociation free energy (BDFE) and free energy of disproportionation (derived from $E_{1/2}$ values).[36] From this analysis we estimate that thermal H_2 release is endergonic, by 8.2 kcal/mol for $\mathbf{1H}^+$ and by 2.2 kcal/mol for $\mathbf{2H}^+$ (see Supporting Information section II). Photoexcitation is therefore driving thermodynamically unfavorable reactions. Yet, when the light is turned off, the reaction does not rapidly revert, despite the reverse H_2 splitting reactions being exergonic. It is known that these nickel complexes face a high kinetic barrier for thermal heterolytic H_2 splitting in concert with a base, taking weeks to proceed to in acetonitrile solvent.[37] The effect is particularly pronounced in acetonitrile, where solvent ligation inhibits coordination of H_2 to the nickel center.[44] The high thermal barrier for H_2 splitting is therefore an essential feature of the light-driven H_2 evolution reactivity.

H_2 Evolution in the Presence of Acids. Photoelectrocatalysis would require a proton source, so we next examined photochemical H_2 evolution from nickel hydrides in the presence of molecular acids. An ideal acid would be sufficiently acidic to protonate a nickel(0) species and generate $\mathbf{1H}^+$ and $\mathbf{2H}^+$ but not so acidic that H_2 production occurs in the dark. Thermodynamic analyses were used to predict appropriate acids. All acids described were used in buffers of acid and base (herein written as X:Y mM buffer, which represents a buffer containing X mM acid, HB^+, and Y mM base, B).

The known hydricity values of $\mathbf{1H}^+$ ($\Delta G°_{H-}$ = 49.9 kcal/mol) and $\mathbf{2H}^+$ ($\Delta G°_{H-}$ = 55.3 kcal/mol)[45] in MeCN allowed us to predict which acids would produce H_2 in the dark. For $\mathbf{1H}^+$, dark H_2 evolution was predicted to be thermodynamically feasible for acids with pK_a < 19.1 in MeCN; for $\mathbf{2H}^+$, stronger acids are needed, pK_a < 15.2 (see Supporting Information section II for derivation).[46] Figure 3 presents the free energy of the reaction of each nickel hydride with three particular acids to release H_2. Table S4 summarizes all of the NMR-scale photochemical H_2 evolution data in the presence of acid. Treating 5 mM (2.5 μmol) solutions of $\mathbf{1H}^+$ or $\mathbf{2H}^+$ with a strongly acidic anilinium buffer (25:2.5 mM $[PhNH_3][BF_4]$, pK_a = 10.6)[47] generated ca. 2.5 μmol of H_2 and ca. 2.5 μmol of

https://doi.org/10.1021/jacs.1c10628
J. Am. Chem. Soc. XXXX, XXX, XXX−XXX

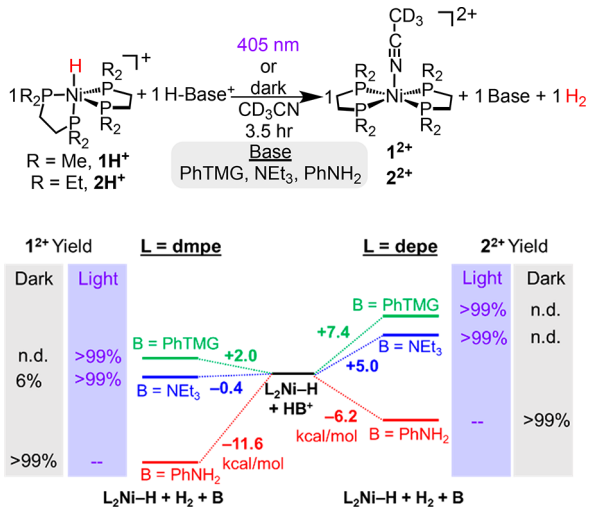

Figure 3. Top: the reactivity of $\mathbf{1H}^+$ or $\mathbf{2H}^+$ with various acids in the light or in the dark. Bottom: the free energy of dark H_2 evolution for Ni bis(diphosphine) hydrides (L_2Ni-H, where L = dmpe or depe) with three different acids, showing the yield of the nickel dicationic species, $\mathbf{1}^{2+}$ or $\mathbf{2}^{2+}$.

the corresponding nickel(II) complexes $\mathbf{1}^{2+}$ or $\mathbf{2}^{2+}$ after less than 45 min in the dark. The stoichiometry of 1 equiv of H_2 from 1 equiv of Ni hydride contrasts with the 1/2 equiv of H_2 generated from photolysis of 1 equiv of Ni hydride in the absence of added acid. Conversely, when solutions containing 2.5 μmol of $\mathbf{1H}^+$ or $\mathbf{2H}^+$ (5 mM Ni) are treated with the more weakly acidic 2-phenyl-1,1,3,3-tetramethylguanidinium buffer (25:2.5 mM [H-PhTMG][PF_6], pK_a = 20.6),[48] there is no observable reaction over 3.5 h in the dark. This result is consistent with the prediction that the H_2 evolution reaction would be endergonic (Figure 3). Triethylammonium has an intermediate pK_a and was predicted to react with $\mathbf{1H}^+$ but not with $\mathbf{2H}^+$. Indeed, 5 mM solutions of $\mathbf{1H}^+$ react with triethylammonium buffer (25:2.2 mM [H-NEt_3][PF_6], pK_a = 18.8)[48] to slowly produce ~6% yield of $\mathbf{1}^{2+}$ after 3.5 h in the dark, while $\mathbf{2H}^+$ did not react under the same reaction conditions.

The thermally endergonic reactions of Figure 3 can be driven by using visible light energy. Illumination of 5 mM (2.5 μmol) solutions of $\mathbf{1H}^+$ or $\mathbf{2H}^+$ in the presence of the above H-PhTMG$^+$ buffer solutions at 405 nm for 3.5 h resulted in ca. 2.5 μmol of H_2 and ca. 2.5 μmol of the dicationic nickel(II) species $\mathbf{1}^{2+}$ and $\mathbf{2}^{2+}$. Quantitative H_2 evolution was also observed upon illumination of the nickel hydrides in the presence of H–NEt_3^+ buffer. The stoichiometry of 1 equiv of H_2 from 1 equiv of Ni hydride is consistent with one hydrogen atom deriving from the Ni hydride and the other from the organic acid.

The initial reactivity studies demonstrate photochemical H_2 evolution from well-defined nickel hydrides with visible light. Purely thermal H_2 evolution reactions of these complexes require quite strong acids, while photochemical H_2 release proceeds smoothly even with very weak acids—or with no acid at all. A thermodynamic analysis confirms that visible light is driving thermally endergonic H_2 evolution from $\mathbf{1H}^+$ or $\mathbf{2H}^+$ with H-PhTMG$^+$ (Figure 3). Thus, *dark electrocatalysis* with these complexes would require strong acids such as anilinium, but *photoelectrochemical catalysis* might be possible even with very weak acids (pK_a values around 23). The ability to utilize visible light to drive H_2 evolution with very weak acids can dramatically lower the electrochemical overpotential requirements for catalysis, as we will discuss later. First, we wanted to understand the mechanism of this unusual example of light-driven H_2 evolution from a first-row transition metal hydride.

Origins of Photochemical Activity. Initial studies focused on understanding the reactivity of the excited state. We considered three broad possibilities, based on prior studies of transition metal hydride photochemistry: (A) a bimolecular reaction between the nickel hydride excited state and an acid buffer component, (B) a bimolecular reaction between the nickel hydride excited state and another ground state nickel hydride (self-quenching), or (C) a unimolecular reaction of the nickel hydride excited state.

We set out to distinguish between these reaction pathways, starting with characterization of the excited state. The UV–vis spectrum of the hydride complex with methyl substituents, $\mathbf{1H}^+$, has a feature with λ_{max} of 336 nm (ε = 1480 M^{-1} cm^{-1}) and a shoulder around 420 nm (ε = 543 M^{-1} cm^{-1}) (Figure 4). A similar spectrum is observed for ethyl-substituted hydride

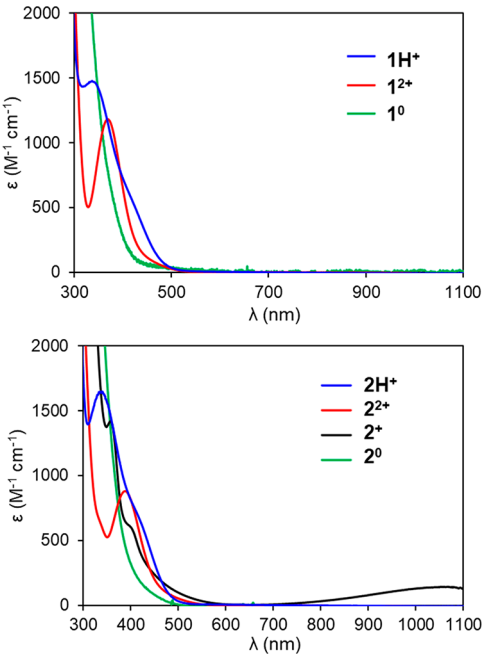

Figure 4. Top: UV–vis spectra of $\mathbf{1H}^+$ (blue), $\mathbf{1}^{2+}$ (as BF_4^- salt, red), and $\mathbf{1}^\circ$ (green) in MeCN. Bottom: UV–vis spectra of $\mathbf{2H}^+$ (blue), $\mathbf{2}^{2+}$ (as BF_4^- salt, red), $\mathbf{2}^+$ (black), and $\mathbf{2}^\circ$ (green) in MeCN.

$\mathbf{2H}^+$: λ_{max} = 337 nm (ε = 1650 M^{-1} cm^{-1}) and 420 nm shoulder (ε = 650 M^{-1} cm^{-1}) (Figure 4). The 405 nm illumination wavelength needed for photochemical H_2 release could plausibly excite either of the optical transitions at the edge of the visible region (wavelength-dependent H_2 evolution is presented below).

The hydride complexes $\mathbf{1H}^+$ and $\mathbf{2H}^+$ are more strongly absorbing around 400 nm than the nickel products of photochemical H_2 evolution as compared in Figure 4. While the nickel(II) complexes ($\mathbf{1}^{2+}$ and $\mathbf{2}^{2+}$) and the nickel(0) complex $\mathbf{1}^\circ$ have qualitatively similar absorption spectra compared to the hydride, the spectrum of the nickel(I) complex $\mathbf{2}^+$ contains a distinctive near-IR feature centered at ~1050 nm in addition to features in the UV region. Similar near-IR absorbances have been observed for other bis-

https://doi.org/10.1021/jacs.1c10628
J. Am. Chem. Soc. XXXX, XXX, XXX–XXX

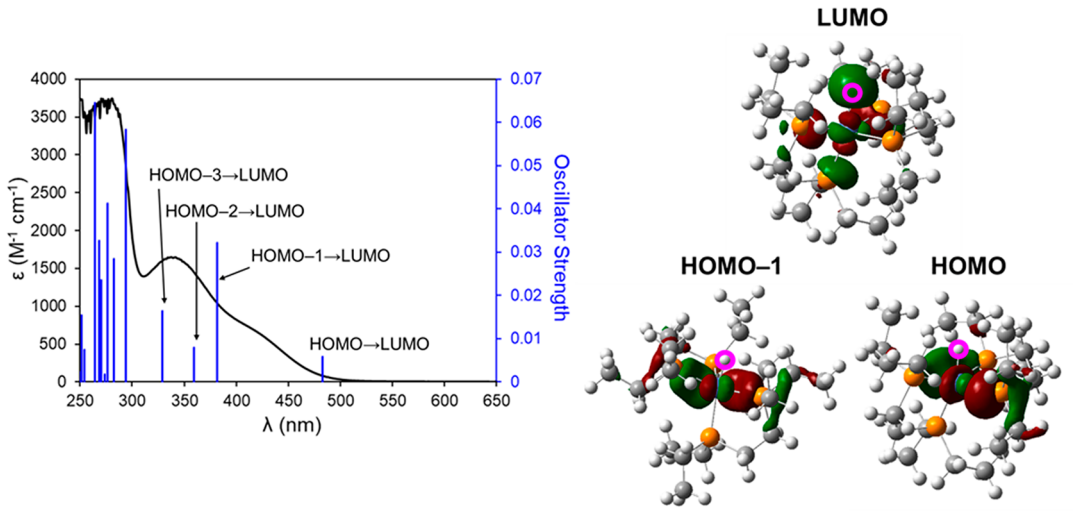

Figure 5. Left: experimental UV−vis spectrum (black line) and calculated excitations (blue lines) for $\mathbf{2H}^+$. Right: calculated orbitals involved in the HOMO−1, HOMO, and LUMO of $\mathbf{2H}^+$, with pink circles around the hydride ligand (right).

(diphoshine) Ni^I complexes.[43] Spectroelectrochemical monitoring of an electrolytic reduction of $\mathbf{2}^{2+}$ in MeCN at approximately −1.2 V vs $Fc^{+/0}$ passed ca. 1.2 e^- per Ni center and gave rise to a UV−vis spectrum analogous to that of independently isolated $\mathbf{2}^+$ (Figure S87).

The nature of the electronic transitions of the two hydride complexes was probed by using time-dependent density functional theory (TD-DFT). The calculated structures of $\mathbf{1H}^+$ and $\mathbf{2H}^+$ both showed distorted trigonal-bipyramidal geometry similar to that observed in the X-ray diffraction study of $\mathbf{2H}^+$ (Figure 5).

For $\mathbf{1H}^+$, the lowest energy feature (483 nm) represents a HOMO → LUMO transition, and the second-lowest (384 nm) represents the HOMO−1 → LUMO. An important insight from TD-DFT is that excitation of either of the two lowest energy transitions should give rise to the same electronic excited state (Figure S93). The HOMO and HOMO−1 both have primarily Ni−P σ^* character. The LUMO in $\mathbf{1H}^+$ features a significant degree of Ni−H σ^* character between the Ni d_{z^2} and H s orbitals, hinting at a possible homolytic or dissociative photochemical pathway. Similar results are seen for $\mathbf{2H}^+$ (Figure 5), indicating a similar origin for photochemical reactivity of these complexes.

To further probe the reactivity of the excited state, photoluminescence and transient absorption spectroscopy experiments were performed. No photoluminescence was detected upon excitation of acetonitrile solutions of $\mathbf{1H}^+$ or $\mathbf{2H}^+$ with either continuous wave or pulsed laser light at 25 or 0 °C. Attempts to detect the metal hydride complexes in their excited states by using nanosecond transient absorption spectroscopy were also unsuccessful, with complete relaxation having occurred within the laser pulse.

Ultrafast transient absorption spectroscopy studies proved more fruitful. Excitation of either $\mathbf{1H}^+$ or $\mathbf{2H}^+$ at 400 nm produced transient features spanning the entire visible region, with peak maxima at 480 and 488 nm, respectively. Single wavelength analyses were fit to a biexponential decays, with one subpicosecond component and one slower time component (~7−8 ps for $\mathbf{1H}^+$ and ~26−30 ps for $\mathbf{2H}^+$). Near-IR ultrafast studies showed broad features with lifetimes in good agreement with the longer decay component of the visible absorbance. The data for $\mathbf{1H}^+$ are presented in Figures S60 and S63, while the data for $\mathbf{2H}^+$ are shown in Figure 6.

The transient absorption studies are consistent with photoexcitation accessing a short-lived singlet excited state

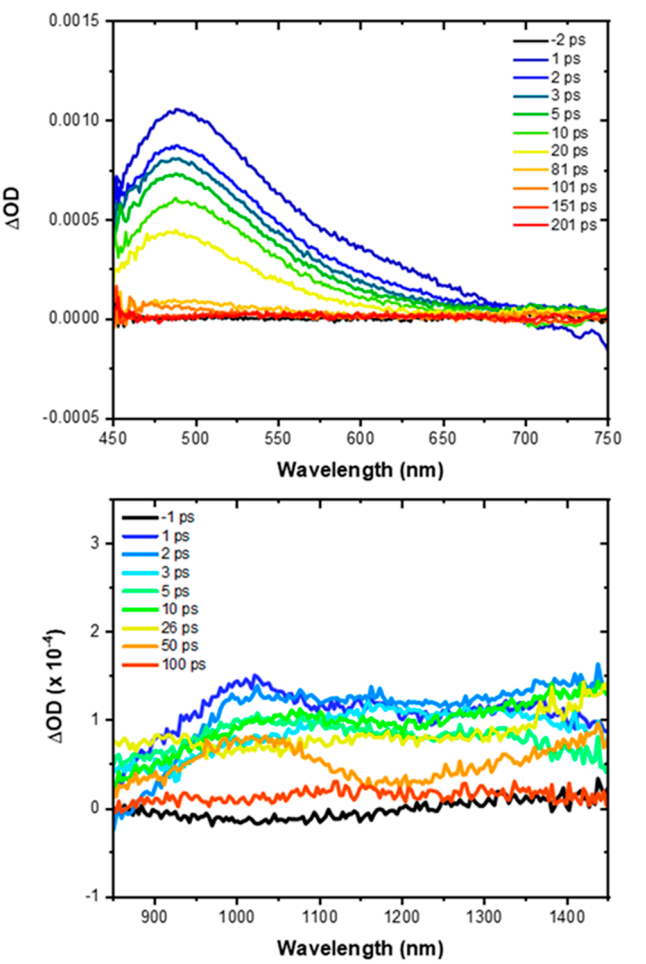

Figure 6. Ultrafast transient absorption (UFTA) spectroscopy of 0.6 mM $\mathbf{2H}^+$ in the visible (top) and near-IR (bottom) regions following 400 nm pulsed laser excitation in MeCN (105 fs fwhm, 1.0 mJ/pulse).

https://doi.org/10.1021/jacs.1c10628
J. Am. Chem. Soc. XXXX, XXX, XXX−XXX

with a high-degree of Ni−H σ^* antibonding character. Sharpening of the transient absorption in the visible region (ca. 500 nm) over time is consistent with vibrational cooling of a singlet excited state (Figure S72). The spectral features of the ground state are restored within ca. 80 ps, and the difference spectrum expected if $\mathbf{2}^+$ was formed is not observed (Figure S73), consistent with minimal net photochemistry with each laser shot. Yet, the presence of near-IR absorbances in the excited states of $\mathbf{1H}^+$ and $\mathbf{2H}^+$, reminiscent of the ground state spectrum of the nickel(I) complex $\mathbf{2}^+$, may reflect an increase in Ni−H σ^* character in the excited state as indicated by TD-DFT.

A lifetime of only a few picoseconds is too short to allow diffusional bimolecular reactions: the excited state would fully relax before it could encounter another nickel hydride or an acid source. This rules out bimolecular reactions of the nickel hydride excited state with acid buffer components or with another ground state nickel hydride complex (self-quenching). The short lifetimes and lack of observed photoproducts instead indicate that a *unimolecular* photochemical process occurs with relatively low photochemical quantum yield. With computational and experimental evidence indicating Ni−H bond weakening in the excited state, a plausible mechanism would involve Ni−H homolysis in excited state to release a (presumably solvent-stabilized) hydrogen atom. In the following sections, additional mechanistic studies provide further evidence for this initial step as well as the following processes along the path that ultimately results in H−H bond formation.

Probing the Mechanism: Photochemical Quantum Yields of H_2. To further probe the H_2 evolution mechanism, photochemical quantum yield measurements varying nickel hydride concentration, acid concentration, and isotopic composition were carried out. To determine the photochemical quantum yield of H_2, Φ_{H2}, an initial rates kinetic analysis was performed. The rate of H_2 release under continuous illumination was determined based on the nickel hydride consumption at less than 10% conversion, with reaction progress monitored by UV−vis spectroscopy. GC headspace measurements showed that the yield of H_2 aligned with the expected stoichiometries of Ni−H consumption by UV−vis spectroscopy (see Supporting Information section V for details).

Without any added acid, the photochemical quantum yield for H_2 evolution varied from approximately 0.003 to 0.015 as the nickel hydride complex concentration increased from 0.5 mM to 5 mM for both $\mathbf{1H}^+$ and $\mathbf{2H}^+$ (Figure 7, Tables S5 and S9). The hydride complex with ethyl substituents, $\mathbf{2H}^+$, had slightly higher Φ_{H2} at all concentrations studied. A positive dependence on nickel concentration is not unexpected given that two nickel hydrides are needed to form 1 equiv of H_2. Although the nickel concentration dependence could conceivably be attributed to excited state quenching by another nickel hydride, the transient absorption spectroscopy studies essentially ruled out such bimolecular pathways; instead, it is more likely that a second nickel hydride reacts with a photogenerated species in a subsequent thermal reaction.

Modulating the photon flux by changing the lamp power did not result in any change in Φ_{H2} for either $\mathbf{1H}^+$ or $\mathbf{2H}^+$ (Figures S58 and S59, Tables S6 and S10), consistent with a photochemical process driven by a single photon absorption event. With TD-DFT data suggesting two viable transitions to reach the same excited state (*vide supra*), an excitation

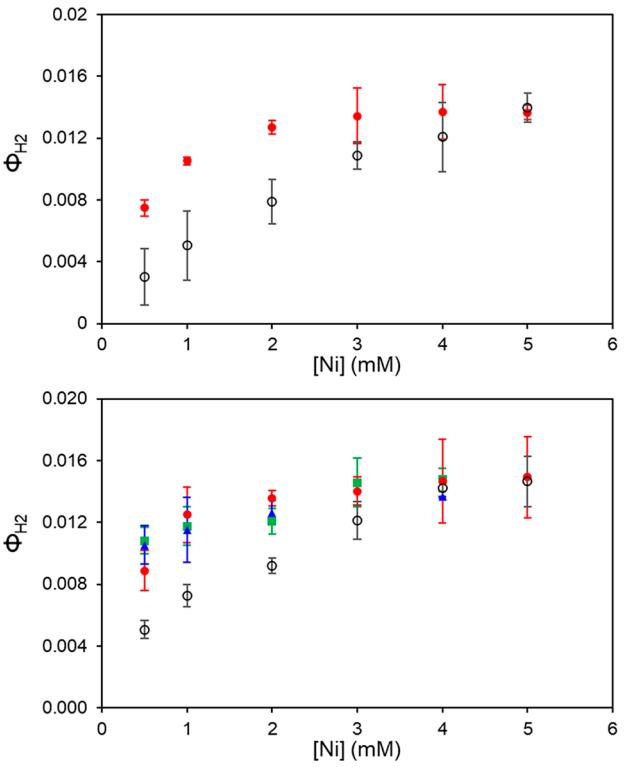

Figure 7. Top: the quantum yield of H_2 evolution (Φ_{H2}) from $\mathbf{1H}^+$ as a function of Ni concentration in MeCN under 405 nm illumination, as determined by UV−vis spectroscopy. Black open circles represent reactions in the absence of acid, and red circles represent reactions containing 25:2.2 mM H-PhTMG$^+$. Bottom: the quantum yield of H_2 evolution (Φ_{H2}) from $\mathbf{2H}^+$ in the presence of acid as a function of nickel concentration in MeCN under 405 nm illumination, as determined by UV−vis spectroscopy. Black open circles represent reactions in the absence of acid, red circles represent reactions containing 25:2.5 H-PhTMG$^+$, blue triangles represent reactions containing 50:5 H-PhTMG$^+$, and green squares represent reactions containing 25:2.5 H-NEt_3^+.

wavelength dependence study was performed. Under lower-energy 443 nm illumination, both $\mathbf{1H}^+$ and $\mathbf{2H}^+$ showed comparable Φ_{H2} as under 405 nm illumination (Tables S7 and S11), suggesting that either transition successfully activates the photochemical reaction. The addition of electrolyte (tetrabutylammonium hexafluorophosphate, [TBA][PF_6]) also had no impact on the quantum yield, consistent with a homolytic mechanism without a significant change in localized charge in the transition state.

In the presence of acids, the reaction stoichiometry changes such that each nickel hydride can produce a total of 1 equiv of H_2 (Scheme 1) rather than 0.5 equiv of H_2 in the absence of acid. For complex $\mathbf{1H}^+$, the H_2 quantum yields in the presence of 25:2.5 mM H-PhTMG$^+$ buffer were within error of those without acid at nickel concentrations above 3 mM. At lower concentrations, however, the quantum yield for H_2 was higher with acid than without (Figure 7 and Table S8).

When $\mathbf{2H}^+$ was photolyzed in the presence of 25:2.5 mM H-PhTMG$^+$, significant amounts of $\mathbf{2}^+$ were observed as an intermediate alongside formation of the final product $\mathbf{2}^{2+}$. Accordingly, the amount of H_2 detected by headspace GC analysis was no longer 1:1 with consumption of $\mathbf{2H}^+$, nor with the appearance of $\mathbf{2}^{2+}$. Only after allowing the cuvette to sit protected from light for 15 min, at which time $\mathbf{2}^+$ was

https://doi.org/10.1021/jacs.1c10628
J. Am. Chem. Soc. XXXX, XXX, XXX−XXX

completely consumed and the concentrations of $\mathbf{2H}^+$ and $\mathbf{2}^{2+}$ both increased, did the yield of H_2 align with the expected stoichiometry (Figure S55). The intermediacy of $\mathbf{2}^+$ is consistent with the mechanism of Scheme 2, wherein

Scheme 2. Proposed Role of Disproportionation in Photochemical H_2 Evolution from L_2NiH^+ (L = dmpe, depe) in the Presence of Acid

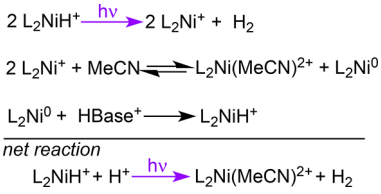

photochemical H_2 evolution from $\mathbf{2H}^+$ initially forms $\mathbf{2}^+$ (as observed without added acid), which undergoes endergonic disproportionation to Ni^{II} and Ni^0 species before the latter is protonated to re-form 1/2 equiv of $\mathbf{2H}^+$.

After properly accounting for the presence of $\mathbf{2}^+$ during photolysis in the presence of acid (see Supporting Information section V for details), the quantum yield of H_2 was found to be similar to that without acid at nickel concentrations >3 mM, reaching a maximum Φ_{H2} of 0.015 (Figure 7 and Table S13). The same Φ_{H2} values were obtained at all Ni concentrations even when the concentration of H-PhTMG$^+$ was doubled or when the stronger acid H-NEt$_3^+$ was utilized (Figure 7). This data confirms that the photochemistry is independent of acid, consistent with the acid serving to regenerate 1/2 equiv of $\mathbf{2H}^+$ in the last step of Scheme 2.

The observation of both $\mathbf{2H}^+$ and $\mathbf{2}^+$ at intermediate times during photolysis in the presence of acid suggests that the disproportionation/protonation sequence of Scheme 2 is occurring at a similar rate to the photochemical H_2 evolution process. Further support comes from electrochemical studies. A pseudo-first-order rate constant for protonation of $\mathbf{2}^\circ$ with H-PhTMG$^+$, $k_{prot} \approx 1\ s^{-1}$, was estimated by cyclic voltammetry (CV, 1 mM $\mathbf{2}^{2+}$ and 100:10 mM H-PhTMG$^+$, Figures S84 and S85). While k_{prot} is much larger than the pseudo-first-order rate constant extracted from the initial rates measurements photochemical H_2 evolution from $\mathbf{2H}^+$ and H-PhTMG$^+$ (ca. 0.002 s^{-1} with 1 mM $\mathbf{2H}^+$ and 25:2.5 mM H-PhTMG$^+$), the ca. 3 kcal/mol endergonic disproportionation would substantially slow the rate of hydride regeneration.

Taken together, the various quantum yield studies further support an initial homolysis event from the nickel hydride excited state, followed by reaction of (solvent-associated) H· with another nickel hydride complex to produce H_2. The subsequent steps involving protonation (or disproportionation followed by protonation) occur at a similar rate as the photochemistry under these conditions.

Probing the Mechanism: Isotopic Labeling and Kinetic Studies. To probe the mechanism of H−H bond formation, isotopic labeling studies were performed. Given that the quantum yield studies indicated that the photochemical mechanism was the same with and without acid, we expected that hydrogen atoms released by a homolysis pathway would react with a second nickel hydride complex to H_2, HD, and D_2 according to Scheme 3. An *operando* photolysis experiment was designed to track the isotopologues of dihydrogen over time during illumination of $\mathbf{2H}^+$ in the presence of acid.

Scheme 3. Proposed Reaction of $[L_2Ni\text{-}H]^+$ (L = depe) with a Deuterated Acid (D-PhTMG$^+$)

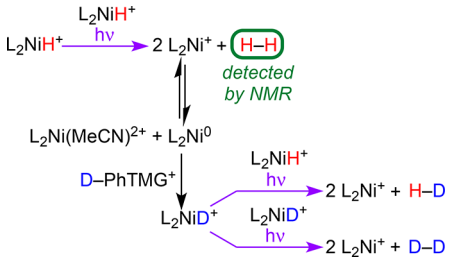

A solution of $\mathbf{2H}^+$ and D-PhTMG$^+$ (25:2.5 mM buffer) was illuminated with 390 nm light by using a fiber optic in the inner tube of a coaxial NMR tube during spectral acquisition. Upon illumination over 30 min, ca. 80% of $\mathbf{2H}^+$ was consumed, with ^{1}H NMR spectral evidence for the concomitant formation of $\mathbf{2}^{2+}$ and $\mathbf{2D}^+$ alongside protio H_2 (Figures S29−S32). The broadness around 1.8 ppm and imperfect mass balance when summing the nickel(II) species suggest that nickel(I) complex $\mathbf{2}^+$ is present as an intermediate, as observed in UV−vis kinetics above. The formation of H_2 establishes that each hydrogen atom originates from $\mathbf{2H}^+$. Mechanisms involving (solvent-associated) H$^\bullet$ directly reacting with the organic acid are also ruled out because this would produce HD as the sole product. According to Scheme 3, HD and D_2 should also be formed during the reaction. No HD was detected in the *operando* experiments, which could be attributed to (a) each line of HD having 1/6 the intensity of the H_2 resonance, (b) poor signal/noise ratio due to the coaxial tube holding the fiber-optic bundle, and (c) continual outgassing of hydrogen during acquisition. The amount of HD formed would also depend on the kinetic isotope effect (KIE), with smaller amounts of HD with larger normal primary KIE values.

The KIE of the photolysis step was evaluated from the photolysis of a 2 mM MeCN solution of independently synthesized deuteride $\mathbf{2D}^+$ (93% D) (without added acid) by UV−vis spectroscopy. The ratio of the initial rate of H_2 evolution by $\mathbf{2H}^+$ and $\mathbf{2D}^+$ gave a KIE = 3.4 ± 0.3 (Figure S47 and Table S12). Similar KIE values were obtained by monitoring the conversion of a ca. 1:1 mixture of $\mathbf{2H}^+$:$\mathbf{2D}^+$ by NMR spectroscopy (Figure S42). When $\mathbf{2H}^+$ was photolyzed in the presence of D-PhTMG$^+$, no significant change in initial rate or Φ_{H2} was observed at <10% conversion compared to the reaction with H-PhTMG$^+$ (KIE = 1.0, Figure S48 and Table S13). This is consistent with protonation of $\mathbf{2}^\circ$ not being a major contributor to the overall rate. An isotope effect comparing $\mathbf{2H}^+$ and $\mathbf{2D}^+$ could be due to either Ni−H bond homolysis or the reaction of a hydrogen atom with a nickel hydride to release dihydrogen. We would expect formation of the strong H−H (D−D) bond at the expense of a much weaker Ni−H (Ni−D) bond to encounter an *inverse* isotope effect in most cases, however.[49]

Proposed Mechanism of Photochemical H_2 Evolution. The combined experimental and computational data point to a mechanism for photochemical H_2 evolution, shown in Scheme 4, that starts with excited state homolysis to generate H$^\bullet$, presumably as an adduct with the acetonitrile solvent.[50,51] The H$^\bullet$ can then either recombine with the nickel(I) species or diffuse to react with a nickel(II) hydride complex in its ground state to form the H−H bond and release H_2. In the absence of acid, the nickel product is determined by

https://doi.org/10.1021/jacs.1c10628
J. Am. Chem. Soc. XXXX, XXX, XXX−XXX

Scheme 4. Proposed Mechanism for Photochemical H_2 Evolution from $[L_2NiH]^+$ (L = dmpe, depe)

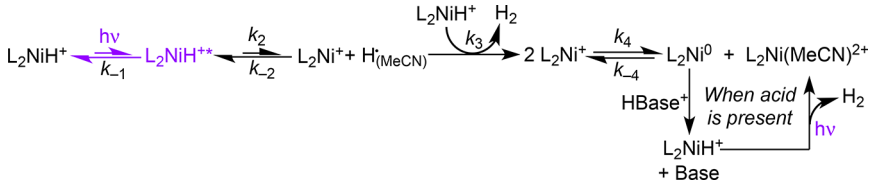

the thermodynamics of disproportionation, with photolysis of the dmpe complex **1H**$^+$ forming a nickel(II)/nickel(0) pair and photolysis of the depe complex **2H**$^+$ producing a nickel(I) complex as the major product. When acid is present in the reaction, protonation of the nickel(0) complex drives disproportionation in both cases, regenerating 1/2 equiv of nickel hydride and funneling back into the same reaction sequence to release a second equivalent of H_2 and the nickel(II) complex as the product.

The mechanism of Scheme 4 is supported by (a) the <30 ps excited state lifetime, which can only support unimolecular photochemical pathways, (b) the large normal primary KIE indicating M−H bond-breaking in the rate-determining step(s), (c) the modest dependence on nickel concentration, consistent with a competition between H· reaction with a nickel hydride to release H_2 evolution and H$^•$ reaction with Ni^I to regenerate the starting hydride, and (d) TD-DFT showing a high degree of Ni−H σ^* antibonding character in the orbital accessed upon photoexcitation and nearly identical quantum yields independent of acid identity or concentration, as expected if the role of acid is to regenerate hydride and shift the overall stoichiometry. Further support for the mechanism of Scheme 4 comes from a kinetic simulation, which qualitatively reproduces the observed nickel concentration dependence of photochemical H_2 release from both **1H**$^+$ and **2H**$^+$ (see Supporting Information section IX). The light-induced Ni−H bond homolysis proposed here is distinct from the photochemical pathway proposed for NiH(N-(CHCHP^{t}Bu$_2$)$_2$), where initial N−H reductive elimination to form a nickel(0) species was invoked.[22]

Additional support for a homolytic hydrogen atom transfer mechanism comes from reactions of **2H**$^+$ with H$^•$ acceptors. Photolysis of 5 mM **2H**$^+$ and 25 mM TEMPO$^•$ produced 4.8 mM of TEMPO−H (0.96 equiv relative to **2H**$^+$) as well as **2**$^+$ (Scheme 5). The same reaction, but with the addition of 25:2.5 mM H-PhTMG$^+$ buffer, produced 7.7 mM TEMPO-H (1.5 equiv relative to **2H**$^+$) and 5 mM **2**$^{2+}$. Similar to the H_2 evolution reactions, the addition of acid allows for the maximum yield of product to double (up to 2 equiv of TEMPO-H formed) due to the regeneration of **2H**$^+$ according to Scheme 2 (above). Despite the dark reaction being favorable by ca. 10 kcal/mol,[52,53] no reactivity with TEMPO· was observed in the dark with or without acid. No H_2 was detected in these experiments, indicating a striking shift from H_2 evolution photochemistry to organic photochemical HAT reactivity.

Benzene was then employed as a much weaker acceptor.[54] No reaction between **2H**$^+$ and C_6D_6 was observed in the dark. After 5 mM **2H**$^+$ was photolyzed for 3.5 h at 405 nm in CD_3CN containing 500 mM C_6D_6, NMR spectroscopy revealed a growth in the C_6D_5H resonance corresponding to an ∼4 mM increase in its concentration (0.82 equiv relative to **2H**$^+$), along with >95% conversion of **2H**$^+$ to **2**$^+$ (Scheme 5). In a separate experiment, the reaction was monitored by

Scheme 5. Photochemical Reactions of 2H$^+$ with TEMPO$^•$ and Benzene

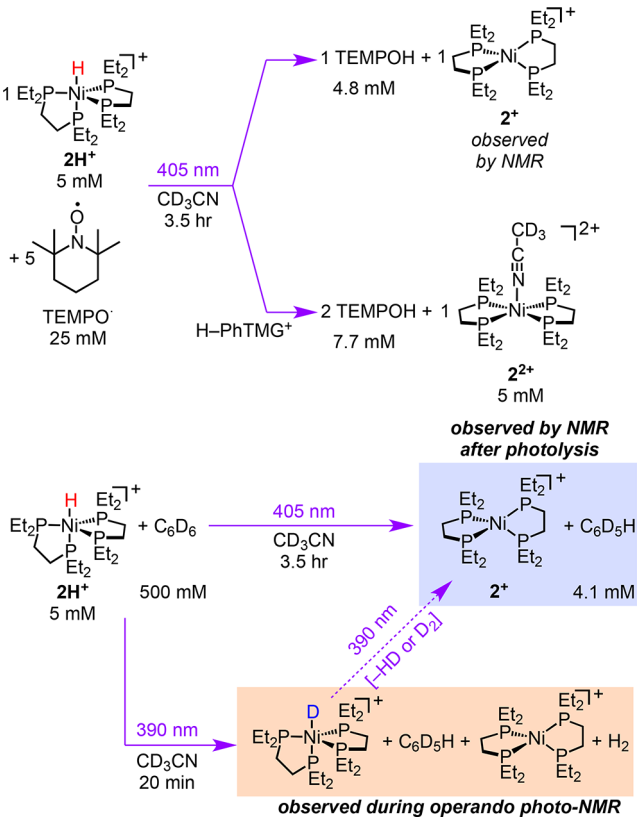

operando NMR spectroscopy during photolysis at 390 nm, which revealed a steady increase in the C_6D_5H resonance was observed alongside formation of **2D**$^+$ (along with some H_2 evolution and broad features consistent with **2**$^+$, Figures S37−S40). The observation of **2D**$^+$ as an intermediate supports the hypothesis of H/D exchange via photoinduced HAT from **2H**$^+$ to C_6D_6 to form **2**$^+$ and $C_6D_6H^•$, which can deliver D$^•$ to **2**$^+$ to generate **2D**$^+$ (with **2D**$^+$ eventually converting to **2**$^+$ by photochemical D_2 evolution). Given that $C_6H_7^•$ is estimated to have a bond dissociation enthalpy of only 24 kcal/mol,[54] this result would require extensive weakening of the Ni−H bond (BDFE ca. 60 kcal/mol in the ground state). Indeed, HAT to benzene is consistent with the excited state of **2H**$^+$ undergoing Ni−H homolysis to form free or solvated H$^•$. These findings parallel those from a recent report from Schneider et al. where H/D exchange was observed between a cobalt hydride and C_6D_6.[55] Few examples of light-induced homolysis of a M−H bond to form free H$^•$ have been proposed.[56−62]

Toward Photoelectrocatalytic H_2 Evolution: Thermodynamic Analysis. Having established the viability of light-driven H_2 generation, we focused on integrating the photochemistry with electrochemical hydride regeneration to complete a catalytic cycle. Scheme 6 depicts the major steps

https://doi.org/10.1021/jacs.1c10628
J. Am. Chem. Soc. XXXX, XXX, XXX−XXX

Scheme 6. Comparison of Mechanisms for H_2 Evolution from $2H^+$ in the Dark (Blue) or under Illumination at 405 nm (Purple), Followed by Electrochemical Regeneration of $2H^+$

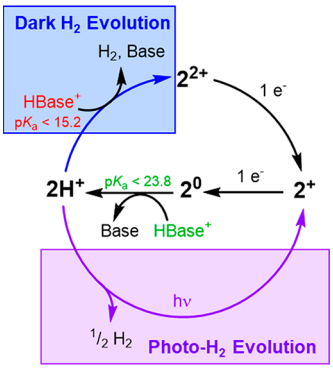

of the proposed mechanism of photochemical H_2 generation by using $\mathbf{2H^+}$ as the example. Although H_2 evolution is a net $2H^+/2e^-$ process, *only one proton transfer step is invoked* in the photoelectrochemical cycle: protonation of a nickel(0) complex generates the nickel(II) hydride which can produce H_2 photochemically by a HAT mechanism. Therefore, photoelectrocatalysis was predicted to proceed smoothly by using any acid that can protonate the nickel(0) intermediate, which would enable catalysis with even very weak acids (pK_a < 23.8 in MeCN for $\mathbf{2H^+}$).[36] This situation is distinct from thermal H_2 electrocatalysis in the dark, which requires two *different* proton transfer reactions: protonation of the nickel(0) intermediate *and* protonation of the less basic nickel(II) hydride species. As shown in Scheme 6, thermal H_2 evolution from nickel(II) hydride complexes involves a proton transfer reaction to release H_2 that depends on the hydricity of the nickel complex as well as the acidity of the proton donor. Based on the hydricity of $\mathbf{2H^+}$,[36] thermal electrocatalysis would require relatively strong acids, with pK_a < 15.2. Complex $\mathbf{1H^+}$ requires pK_a < 24.1 for photoelectrocatalysis and pK_a < 19.1 for dark thermal H_2 evolution (see Supporting Information section II for details). Complex $\mathbf{1^{2+}}$ is expected to follow an analogous cycle, differing mainly in the relatively instability of the nickel(I) intermediate reflected in the presence of a single $2e^-$ reduction in MeCN ($E_{1/2}$ = −1.39 V vs $Fc^{+/0}$), in contrast to $\mathbf{2^{2+}}$, which undergoes two reversible $1e^-$ reductions ($E_{1/2}$ = −1.13 V and $E_{1/2}$ = −1.30 V).[36]

The acid pK_a requirements of a particular catalyst directly influence the electrochemical overpotential that will be expected. The situations of $\mathbf{2^{2+}}$ in the light and the dark are visualized in Figure 8 by using overpotential "maps" that we recently introduced to guide overpotential tuning.[9] In the dark and under illumination, the same applied potential (beyond ca. − 1.3 V for $\mathbf{2^{2+}}$) is required to drive electrocatalysis. In the dark, electrocatalysis with $\mathbf{2^{2+}}$ requires acids of $pK_a \leq 15.2$, which limits the operating conditions and imposes at least +375 mV overpotential. Under illumination, however, weaker acids ($pK_a \leq 23.8$) can be used. Because the thermodynamic requirements for H_2 evolution depend on the acid pK_a, shifting to weaker acids also changes the accessible overpotentials. The nearly 9 unit change in pK_a requirement for thermal vs photochemical catalysis predicts *an improvement of over 500 mV in overpotential under illumination*. Indeed, this analysis predicts catalysis at zero overpotential (or even at an underpotential) would be possible (Figure 8). Similar analysis

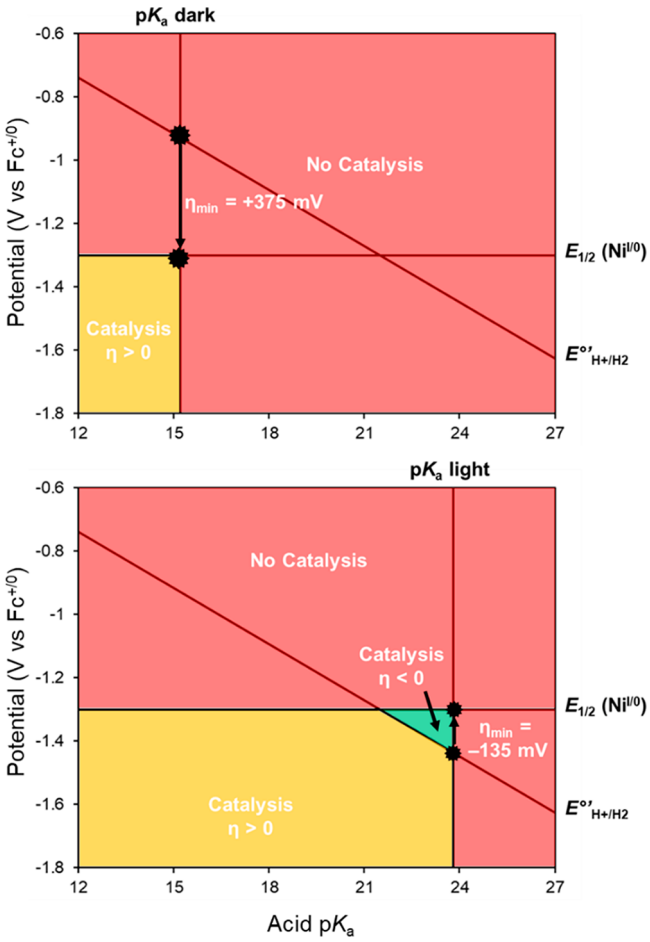

Figure 8. Top: overpotential "map" for the dark electrocatalytic evolution of H_2 from $\mathbf{2^{2+}}$, showing the pK_a requirements for dark H_2 evolution (pK_a dark) and that catalysis is only possible at positive overpotentials ($\eta > 0$). Bottom: overpotential "map" for the photoelectrocatalytic evolution of H_2 from $\mathbf{2^{2+}}$, showing the pK_a requirements for photo-H_2 evolution (pK_a light) and that catalysis is enabled at negative overpotentials ($\eta < 0$). The minimum possible overpotential at $E_{app} = E_{1/2}$ ($Ni^{I/0}$) improves by over 500 mV under illumination compared to dark reactivity.

can be applied to $\mathbf{1^{2+}}$, in which the thermodynamic requirements for photoelectrocatalysis improve by 5 pK_a units and over 300 mV of overpotential compared to dark electrocatalysis (see Supporting Information section II).

Photoelectrochemical Analysis of Nickel Complexes. The foregoing thermodynamic analysis informed our development of a photoelectrocatalytic method for H_2 evolution. Cyclic voltammetry studies of $\mathbf{1^{2+}}$ in the presence of weak acid H-PhTMG$^+$ (100:10 mM) showed an irreversible reduction, consistent with prior reports of hydride generation by electroreduction followed by protonation to form $\mathbf{1H^+}$.[42] Using the stronger acid $PhNH_3^+$ (100:10 mM) resulted in overlap with direct acid reduction. Under illumination, minor current enhancement was observed at slow scan rates, consistent with photoelectrocatalysis for both acids (Figures S75 and S77).[8,9] Cyclic voltammetry of $\mathbf{2^{2+}}$ in the presence of H-PhTMG$^+$ exhibits a quasi-reversible voltammetric response, which enabled the scan-rate dependence studies that provided a rate constant for nickel protonation mentioned above. In the presence of the stronger acid $PhNH_3^+$, $\mathbf{2^{2+}}$ displays a single fully irreversible reduction feature and current enhancement

https://doi.org/10.1021/jacs.1c10628
J. Am. Chem. Soc. XXXX, XXX, XXX−XXX

consistent with dark H_2 evolution. Some photocurrent enhancement consistent with light-driven H_2 evolution nonetheless observed at slow scan rates in the presence of the weaker acid H-PhTMG$^+$ (Figure S79).

Sustained photoelectrocatalytic H_2 evolution was demonstrated by using controlled potential electrolysis (CPE), focusing on **2H**$^+$ because superior overpotentials were predicted and less competition with direct acid reduction was encountered relative to **1H**$^+$. A shutter experiment varying periods of illumination and darkness was performed first. When a solution of **2H**$^+$ with H-PhTMG$^+$ (100:10 mM buffer) was initially electrolyzed in the dark at E_{app} = −1.30 V (η = +120 mV), very little current was passed, indicating that no reaction was occurring (Figure 9). After 5 min, the cell was

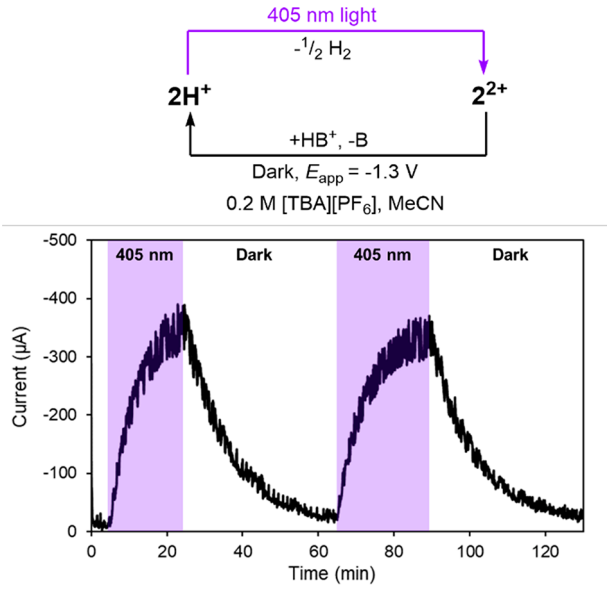

Figure 9. Reaction scheme (top) and current vs time plot (middle) of the shuttered controlled potential electrolysis of 1 mM **2H**$^+$ with 100:10 mM H-PhTMG$^+$ in 0.2 M [TBA][PF_6] in MeCN at E_{app} = −1.30 V vs $Fc^{+/0}$ (η = +120 mV) in the dark (white background) and under 405 nm illumination (purple background). Working electrode = reticulated vitreous carbon, counter electrode = Pt coil, and reference electrode = Ag wire.

exposed to 405 nm light, resulting in a marked current increase indicative of photoelectrocatalytic H_2 evolution. When the light was turned off, the current decayed over several minutes, consistent with dark electrochemical formation of **2H**$^+$. A second shutter sequence yielded almost identical results.

Several photoelectrocatalytic conditions covering a range of overpotentials were examined, with applied potentials chosen based on the relationship to the CV features (Figure 10). For convenience, these experiments started with the dicationic nickel(II) complex **2**$^{2+}$ rather than the hydride complex. When **2**$^{2+}$ was electrolyzed at E_{app} = −1.30 V in the dark with H-PhTMG$^+$ (100:10 mM buffer, η = +120 mV), 1.9 e$^-$ were passed per Ni equivalent to generate **2H**$^+$, after which the measured current dropped to a sustained value of −12 μA (Figure 11). No H_2 was detected by GC analysis of the headspace after electrolysis. Under identical conditions, but with 405 nm illumination, the current leveled off to a higher value of −137 μA. This >10-fold higher current increase under illumination confirms a photoelectrocatalytic reaction, with Faradaic efficiency for H_2 of 101 ± 3% based on headspace GC

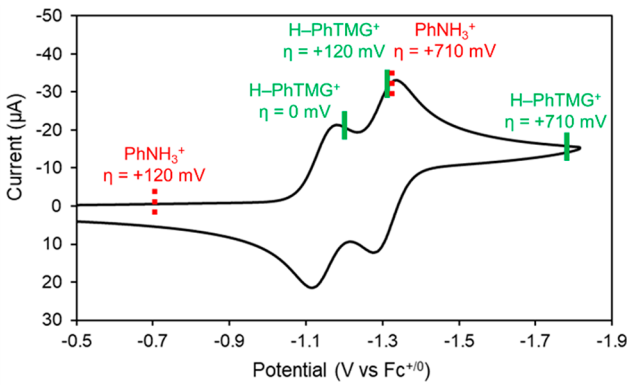

Figure 10. Cyclic voltammogram of 1 mM **2**$^{2+}$ (as BF_4^- salt) in MeCN showing relevant overpotentials for catalysis using 100:10 mM buffers of H-PhTMG$^+$ (green solid) or $PhNH_3^+$ (red dashed).

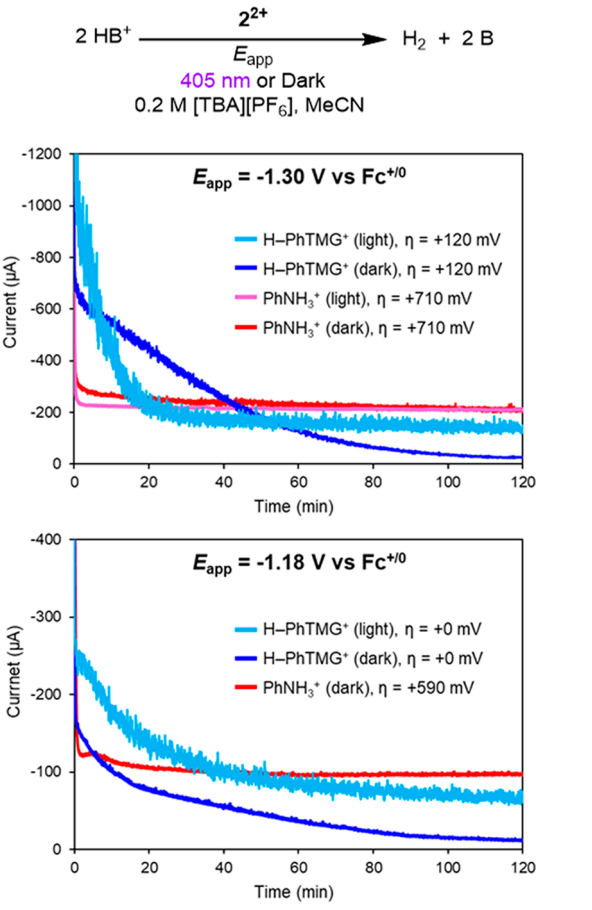

Figure 11. Reaction scheme (top) and current vs time plots for controlled potential electrolysis of 1 mM **2**$^{2+}$ (as BF_4^- salt) with and without illumination in 0.2 M [TBA][PF_6] in MeCN at an applied potential of −1.30 V vs $Fc^{+/0}$ (middle) and at an applied potential of −1.18 V vs $Fc^{+/0}$ (bottom) with 100:10 mM H-PhTMG$^+$ (dark/light blue) or 100:10 mM $PhNH_3^+$ (red/pink). Working electrode = reticulated vitreous carbon, counter electrode = Pt coil, and reference electrode = Ag wire.

analysis. As expected, H_2 evolution in the dark requires the use of a stronger acid: at the same applied potential, E_{app} = −1.30 V, electrolysis of **2**$^{2+}$ with $PhNH_3^+$ (100:10 mM buffer) in the dark evolves H_2 with sustained current of −210 μA (Faradaic efficiency for H_2 of 102 ± 3%). No current enhancement was

https://doi.org/10.1021/jacs.1c10628
J. Am. Chem. Soc. XXXX, XXX, XXX−XXX

observed under photolysis by using the same experimental conditions. This dark H_2 evolution reaction with strong acid has only slightly higher sustained currents than the photoelectrochemical variant with weak acid yet operates at a dramatically higher overpotential, η = +710 mV (vs η = +120 mV with weak acid under illumination). Attempts to drive H_2 evolution at low overpotential in the dark with the stronger acid $PhNH_3^+$ failed: electrolysis at an overpotential of η = +120 mV (E_{app} = −0.71 V) gave no evidence of electrochemical activity, as expected based on the location of the reduction features of $\mathbf{2}^{2+}$.

We hypothesized that H_2 evolution with H-PhTMG$^+$ at even lower overpotential would be possible. In the photochemical studies of $\mathbf{2H}^+$ described above, disproportionation of $\mathbf{2}^+$ was invoked in the presence of acid as a route to the product $\mathbf{2}^{2+}$. During electrolysis at sufficiently negative applied potentials, any $\mathbf{2}^+$ would presumably be rapidly reduced to $\mathbf{2}°$. At less negative potentials, however, $\mathbf{2}^+$ could disproportionate to $\mathbf{2}°$ and $\mathbf{2}^{2+}$; equilibrium amounts of $\mathbf{2}°$ could be protonated to generate $\mathbf{2H}^+$, and the $\mathbf{2}^{2+}$ could be reduced to $\mathbf{2}^+$ to continue disproportionation, enabling photoelectrocatalysis at the *first* reduction feature. As shown in Figure 10, the $Ni^{II/I}$ couple ($E_{1/2}$ = −1.13 V) aligns nicely with the thermodynamic potential for H_2 evolution under the chosen conditions with H-PhTMG$^+$ ($E^{\circ\prime}_{H+/H2}$ = −1.18 V). Under these conditions with illumination at 405 nm, a current of −67 μA was sustained, and H_2 was produced in 100 ± 4% Faradaic efficiency, demonstrating H_2 evolution catalysis at zero overpotential (Figure 11). At the same applied potential, dark electrocatalysis with the stronger acid $PhNH_3^+$ requires nearly 600 mV of overpotential (η = +590 mV).

The turnover number (TON) for H_2 evolution produced during CPE can be determined based on the moles of H_2 detected in the headspace, divided by the total moles of nickel complex in the cell. In the presence of H-PhTMG$^+$ and with E_{app} = −1.30 V vs $Fc^{+/0}$, the H_2 yields gave a TON = 12 over the course of 2 h. This corresponds to a total TOF of 0.002 s^{-1}, which aligns with the first-order rate constant extracted from initial rates measurements of photochemical H_2 release from $\mathbf{2H}^+$ and H-PhTMG$^+$—also estimated at 0.002 s^{-1}. This suggests that the limiting reaction in photoelectrocatalysis is the photochemical H_2 evolution step and that the hydride $\mathbf{2H}^+$ is generated at the surface of the electrode before moving into the bulk solution to undergo the photochemical reaction.

Comparisons between photoelectrocatalysts are difficult, but the rate constant is lower than iridium-based catalysts,[8,9] which we attribute to the lower quantum yield for H_2 formation. The photocurrent enhancement was similar to previously reported molecular photoelectrocatalysts,[8,9] however, showing that 3d transition metal catalysts can indeed carry out sensitizer-free photoelectrocatalysis.

The performance of the present single-component molecular photoelectrocatalyst can also be compared with multicomponent systems composed of a silicon photoelectrode and a surface-anchored molecular catalyst. A leading example uses p-type silicon as the light absorber, with a mesoporous TiO_2 nanoparticle layer on which a phosphonate-decorated P_2N_2-type nickel catalyst is attached. Photoelectrocatalytic H_2 evolution is observed at η = 0 V (no overpotential required) and TOF = 0.007 s^{-1}, proceeding with 76−87% Faradaic efficiency.[35] The present system requires no semiconductor light absorber yet also evolves H_2 at η = 0 V, with TOF = 0.002 s^{-1} and Faradaic efficiency of ca. 100%. This is particularly remarkable when considering that the Si/Ni system utilizes a Ni catalyst with pendent amines designed to maximize H_2 evolution rates, whereas the present system utilizes simple diphosphine ligands that are much slower thermal (dark) H_2 evolution catalysts.

CONCLUSIONS

New photochemical H_2 evolution reactivity of nickel bis(diphosphine) hydride complexes enabled the development of the first molecular photoelectrocatalyst for H_2 evolution based on a first-row transition metal. This first example of visible-light-triggered H_2 evolution from a nickel hydride provided an opportunity for mechanistic studies to help understand the factors that support productive fuel-forming photochemistry in 3d metal complexes. Mechanistic studies are consistent with photoexcitation to generate a short-lived singlet excited state with substantial Ni−H bond weakening, which undergoes Ni−H homolysis to release $H^•$ with low quantum yield. The $H^•$ equivalent can react with another nickel hydride to release H_2, or it can be intercepted with other acceptors such as $TEMPO^•$.

Pairing the new photochemical H_2 release reactivity with known electrochemical nickel hydride generation reactivity enables the first example of a single-component molecular photoelectrocatalyst for H_2 evolution utilizing a first-row transition metal. The distinct mechanism of H_2 release by using requires only very weak acids for catalysis and thus enables light-driven H_2 evolution without any overpotential (at the H^+/H_2 thermodynamic potential). In the dark, H_2 evolves only when strong acids are used, leading to ca. 600 mV higher overpotential to achieve similar rates.

ASSOCIATED CONTENT

Supporting Information

The Supporting Information is available free of charge at https://pubs.acs.org/doi/10.1021/jacs.1c10628.

Experimental details and characterization, determination of quantum yields and lifetimes (PDF)

Accession Codes

CCDC 2113817 contains the supplementary crystallographic data for this paper. These data can be obtained free of charge via www.ccdc.cam.ac.uk/data_request/cif, or by emailing data_request@ccdc.cam.ac.uk, or by contacting The Cambridge Crystallographic Data Centre, 12 Union Road, Cambridge CB2 1EZ, UK; fax: +44 1223 336033.

AUTHOR INFORMATION

Corresponding Author

Alexander J. M. Miller − *Department of Chemistry, University of North Carolina at Chapel Hill, Chapel Hill, North Carolina 27599-3290, United States;* orcid.org/0000-0001-9390-3951; Email: ajmm@email.unc.edu

Authors

Bethany M. Stratakes − *Department of Chemistry, University of North Carolina at Chapel Hill, Chapel Hill, North Carolina 27599-3290, United States*

Kaylee A. Wells − *Department of Chemistry, North Carolina State University, Raleigh, North Carolina 27695-8204, United States;* orcid.org/0000-0002-6870-6574

Daniel A. Kurtz − *Department of Chemistry, University of North Carolina at Chapel Hill, Chapel Hill, North Carolina*

https://doi.org/10.1021/jacs.1c10628
J. Am. Chem. Soc. XXXX, XXX, XXX−XXX

27599-3290, United States; orcid.org/0000-0002-0082-1699

Felix N. Castellano − *Department of Chemistry, North Carolina State University, Raleigh, North Carolina 27695-8204, United States;* orcid.org/0000-0001-7546-8618

Complete contact information is available at: https://pubs.acs.org/10.1021/jacs.1c10628

Notes

The authors declare no competing financial interest.

■ ACKNOWLEDGMENTS

The synthesis, steady-state photochemistry, and electrochemistry work (B.M.S. and A.J.M.M.) was supported by the U.S. Department of Energy, Office of Science, Office of Basic Energy Sciences, under Award DE-SC0014255. The ultrafast transient absorption work was performed (K.A.W. and F.N.C.) at the NCSU Imaging and Kinetic Spectroscopy (IMAKS) Laboratory and was supported by the National Science Foundation (CHE-1955795). The authors thank Andrew Camp for his help with the *in situ* NMR photolysis experiments, Claudio Mastrocinque for his help with photoluminescence spectroscopy, and Michael Mortelliti and Ann Marie May for their help with nanosecond transient absorption spectroscopy.

■ REFERENCES

(1) Brereton, K. R.; Bonn, A. G.; Miller, A. J. M. Molecular Photoelectrocatalysts for Light-Driven Hydrogen Production. *ACS Energy Lett.* **2018**, *3* (5), 1128−1136.

(2) Ziessel, R. Efficient Homogeneous Photochemical Water Gas Shift Reaction Catalysed under Extremely Mild Conditions by Novel Iridium(III) Complexes: $[(^5\text{-}Me_5C_5)Ir(bpy)Cl]^+$, $[(,^5\text{-}Me_5C_5)Ir(bpy)H]^+$, and $[(,^5\text{-}Me_5C_5)Ir(phen)Cl]^+$. *J. Chem. Soc., Chem. Commun.* **1988**, *0*, 16−17.

(3) Youinou, M. T.; Ziessel, R. Synthesis and Molecular Structure of a New Family of Iridium-(III) and Rhodium(III) Complexes: $[((^5\text{-}Me_5C_5)Ir(LL)X]^+$ and $[(^5\text{-}Me_5C_5)Rh(LL)Cl]^+$; LL = 2,2●-Bipyridine or 1,10-Phenanthroline; X = Cl or H. Single Crystal Structures of $[(C^5\text{-}Me_5C_5)Ir(bpy)Cl]Cl$ and $[(d^5\text{-}Me_5C_5)Rh(phen)Cl]ClO_4$. *J. Organomet. Chem.* **1989**, *363* (1−2), 197−208.

(4) Sandrini, D.; Maestri, M.; Ziessel, R. Spectroscopic Behavior of a New Family of Mixed-Ligand Iridium(III) Complexes. *Inorg. Chim. Acta* **1989**, *163* (2), 177−180.

(5) Ziessel, R. Photocatalysis of the Homogeneous Water-Gas Shift Reaction under Ambient Conditions by Cationic Iridium (III) Complexes. *Angew. Chem., Int. Ed. Engl.* **1991**, *30* (7), 844−847.

(6) Caix, C.; Chardon-Noblat, S.; Deronzier, A.; Ziessel, R. Electrochemical Generation of a Metal-Hydride Complex $[(C_5Me_5)Ir(L)H]^+$ (L = 2,2●-Bipyridine). The Electrochemical Behaviour. *J. Electroanal. Chem.* **1993**, *362* (1−2), 301−304.

(7) Ziessel, R. Photocatalysis. Mechanistic Studies of Homogeneous Photochemical Water Gas Shift Reaction Catalyzed under Mild Conditions by Novel Cationic Iridium(III) Complexes. *J. Am. Chem. Soc.* **1993**, *115* (1), 118−127.

(8) Pitman, C. L.; Miller, A. J. M. Molecular Photoelectrocatalysts for Visible Light-Driven Hydrogen Evolution from Neutral Water. *ACS Catal.* **2014**, *4* (8), 2727−2733.

(9) Stratakes, B. M.; Miller, A. J. M. H_2 Evolution at an Electrochemical "Underpotential" with an Iridium-Based Molecular Photoelectrocatalyst. *ACS Catal.* **2020**, *10* (16), 9006−9018.

(10) Rivier, L.; Peljo, P.; Vannay, L. A. C.; Gschwend, G. C.; Méndez, M. A.; Corminboeuf, C.; Scanlon, M. D.; Girault, H. H. Photoproduction of Hydrogen by Decamethylruthenocene Combined with Electrochemical Recycling. *Angew. Chem., Int. Ed.* **2017**, *56*, 2324−2327.

(11) Rivier, L.; Peljo, P.; Maye, S.; Mendez, M. A.; Vrubel, H.; Vannay, L. A. C.; Corminboeuf, C.; Scanlon, M. D.; Girault, H. H. Mechanistic Study on the Photogeneration of Hydrogen by Decamethylruthenocene. *Chem. - Eur. J.* **2019**, *25* (55), 12769−12779.

(12) Huang, J.; Sun, J.; Wu, Y.; Turro, C. Dirhodium(II,II)/NiO Photocathode for Photoelectrocatalytic Hydrogen Evolution with Red Light. *J. Am. Chem. Soc.* **2021**, *143* (3), 1610−1617.

(13) Wilson, A. D.; Newell, R. H.; McNevin, M. J.; Muckerman, J. T.; Rakowski DuBois, M.; DuBois, D. L. Hydrogen Oxidation and Production Using Nickel-Based Molecular Catalysts with Positioned Proton Relays. *J. Am. Chem. Soc.* **2006**, *128* (1), 358−366.

(14) Helm, M. L.; Stewart, M. P.; Bullock, R. M.; DuBois, M. R.; DuBois, D. L. A Synthetic Nickel Electrocatalyst with a Turnover Frequency Above 100,000 s^{-1} for H_2 Production. *Science* **2011**, *333* (6044), 863−866.

(15) McCusker, J. K. Electronic Structure in the Transition Metal Block and Its Implications for Light Harvesting. *Science* **2019**, *363* (6426), 484−488.

(16) Perutz, R. N.; Procacci, B. Photochemistry of Transition Metal Hydrides. *Chem. Rev.* **2016**, *116* (15), 8506−8544.

(17) Geoffroy, G. L.; Wrighton, M. S. *Organometallic Photochemistry*; Academic Press: New York, 1979.

(18) Wang, W.; Rauchfuss, T. B.; Bertini, L.; Zampella, G. Unsensitized Photochemical Hydrogen Production Catalyzed by Diiron Hydrides. *J. Am. Chem. Soc.* **2012**, *134* (10), 4525−4528.

(19) Bertini, L.; Fantucci, P.; De Gioia, L.; Zampella, G. Excited State Properties of Diiron Dithiolate Hydrides: Implications in the Unsensitized Photocatalysis of H_2 Evolution. *Inorg. Chem.* **2013**, *52* (17), 9826−9841.

(20) Frederix, P. W. J. M.; Adamczyk, K.; Wright, J. A.; Tuttle, T.; Ulijn, R. V.; Pickett, C. J.; Hunt, N. T. Investigation of the Ultrafast Dynamics Occurring during Unsensitized Photocatalytic H_2 Evolution by an [FeFe]-Hydrogenase Subsite Analogue. *Organometallics* **2014**, *33* (20), 5888−5896.

(21) Hontzopoulos, E.; Vrachnou-Astra, E.; Konstantatos, J.; Katakis, D. A New Photosensitizer—Catalyst for the Photochemical Cleavage of Water. *J. Photochem.* **1985**, *30* (1), 117−120.

(22) Schneck, F.; Finger, M.; Stuckl, A. C.; Wurtele, C.; Schneider, S.; Ahrens, J.; Schwarzer, D. The Elusive Abnormal CO_2 Insertion Enabled by Metal-Ligand Cooperative Photochemical Selectivity Inversion. *Nat. Commun.* **2018**, *9* (1), 1161.

(23) Heitz, D. R.; Tellis, J. C.; Molander, G. A. Photochemical Nickel-Catalyzed C-H Arylation: Synthetic Scope and Mechanistic Investigations. *J. Am. Chem. Soc.* **2016**, *138* (39), 12715−12718.

(24) Welin, E. R.; Le, C.; Arias-Rotondo, D. M.; McCusker, J. K.; MacMillan, D. W. C. Photosensitized, Energy Transfer-Mediated Organometallic Catalysis through Electronically Excited Nickel(II). *Science* **2017**, *355* (6323), 380−385.

(25) Ting, S. I.; Garakyaraghi, S.; Taliaferro, C. M.; Shields, B. J.; Scholes, G. D.; Castellano, F. N.; Doyle, A. G. 3d-d Excited States of Ni(II) Complexes Relevant to Photoredox Catalysis: Spectroscopic Identification and Mechanistic Implications. *J. Am. Chem. Soc.* **2020**, *142* (12), 5800−5810.

(26) Schneck, F.; Finger, M.; Stuckl, A. C.; Wurtele, C.; Schneider, S.; Ahrens, J.; Schwarzer, D. The Elusive Abnormal CO_2 Insertion Enabled by Metal-Ligand Cooperative Photochemical Selectivity Inversion. *Nat. Commun.* **2018**, *9* (1), 1161.

(27) Klug, C. M.; Cardenas, A. J. P.; Bullock, R. M.; O'Hagan, M.; Wiedner, E. S. Reversing the Tradeoff between Rate and Overpotential in Molecular Electrocatalysts for H_2 Production. *ACS Catal.* **2018**, *8* (4), 3286−3296.

(28) Klug, C. M.; Dougherty, W. G.; Kassel, W. S.; Wiedner, E. S. Electrocatalytic Hydrogen Production by a Nickel Complex Containing a Tetradentate Phosphine Ligand. *Organometallics* **2019**, *38* (6), 1269−1279.

(29) Esswein, A. J.; Nocera, D. G. Hydrogen Production by Molecular Photocatalysis. *Chem. Rev.* **2007**, *107* (10), 4022−4047.

(30) McLaughlin, M. P.; McCormick, T. M.; Eisenberg, R.; Holland, P. L. A Stable Molecular Nickel Catalyst for the Homogeneous Photogeneration of Hydrogen in Aqueous Solution. *Chem. Commun.* **2011**, *47* (28), 7989−7991.
(31) Gross, M. A.; Reynal, A.; Durrant, J. R.; Reisner, E. Versatile Photocatalytic Systems for H_2 Generation in Water Based on an Efficient DuBois-Type Nickel Catalyst. *J. Am. Chem. Soc.* **2014**, *136* (1), 356−366.
(32) Seo, J.; Pekarek, R. T.; Rose, M. J. Photoelectrochemical Operation of a Surface-Bound, Nickel-Phosphine H_2 Evolution Catalyst on p-Si(111): A Molecular Semiconductor|catalyst Construct. *Chem. Commun.* **2015**, *51* (68), 13264−13267.
(33) Rosser, T. E.; Gross, M. A.; Lai, Y.-H.; Reisner, E. Precious-Metal Free Photoelectrochemical Water Splitting with Immobilised Molecular Ni and Fe Redox Catalysts. *Chem. Sci.* **2016**, *7* (7), 4024−4035.
(34) Gross, M. A.; Creissen, C. E.; Orchard, K. L.; Reisner, E. Photoelectrochemical Hydrogen Production in Water Using a Layer-by-Layer Assembly of a Ru Dye and Ni Catalyst on NiO. *Chem. Sci.* **2016**, *7* (8), 5537−5546.
(35) Leung, J. J.; Warnan, J.; Nam, D. H.; Zhang, J. Z.; Willkomm, J.; Reisner, E. Photoelectrocatalytic H_2 Evolution in Water with Molecular Catalysts Immobilised on P-Si via a Stabilising Mesoporous TiO_2 Interlayer. *Chem. Sci.* **2017**, *8* (7), 5172−5180.
(36) Berning, D. E.; Noll, B. C.; DuBois, D. L. Relative Hydride, Proton, and Hydrogen Atom Transfer Abilities of $[HM(Diphosphine)_2]PF_6$ Complexes (M = Pt, Ni). *J. Am. Chem. Soc.* **1999**, *121* (49), 11432−11447.
(37) Curtis, C. J.; Miedaner, A.; Ellis, W. W.; DuBois, D. L. Measurement of the Hydride Donor Abilities of $[HM(Diphosphine)_2]^+$ Complexes (M = Ni, Pt) by Heterolytic Activation of Hydrogen. *J. Am. Chem. Soc.* **2002**, *124* (9), 1918−1925.
(38) Curtis, C. J.; Miedaner, A.; Ciancanelli, R.; Ellis, W. W.; Noll, B. C.; DuBois, M. R.; DuBois, D. L. $[Ni(Et_2PCH_2NMeCH_2PEt_2)_2]^{2+}$ as a Functional Model for Hydrogenases. *Inorg. Chem.* **2003**, *42* (1), 216−227.
(39) Tsay, C.; Yang, J. Y. Electrocatalytic Hydrogen Evolution under Acidic Aqueous Conditions and Mechanistic Studies of a Highly Stable Molecular Catalyst. *J. Am. Chem. Soc.* **2016**, *138* (43), 14174−14177.
(40) Tsay, C.; Ceballos, B. M.; Yang, J. Y. pH-Dependent Reactivity of a Water-Soluble Nickel Complex: Hydrogen Evolution vs. Selective Electrochemical Hydride Generation. *Organometallics* **2019**, *38* (6), 1286−1291.
(41) Stratakes, B. M.; Dempsey, J. L.; Miller, A. J. M. Determining the Overpotential of Electrochemical Fuel Synthesis Mediated by Molecular Catalysts: Recommended Practices, Standard Reduction Potentials, and Challenges. *ChemElectroChem.* **2021**, *8*, 4161.
(42) Miedaner, A.; DuBois, D. L.; Curtis, C. J.; Haltiwanger, R. C. Generation of Metal Formyl Complexes Using Nickel and Platinum Hydrides as Reducing Agents. *Organometallics* **1993**, *12* (2), 299−303.
(43) Bontempelli, G.; Daniele, S.; Favero, G. The Solution State of Nickel(II) and Nickel(I) in the Presence of Diphosphines in Acetonitrile. A Combined Electroanalytical and Spectrophotometric Approach. *Inorg. Chim. Acta* **1984**, *85* (1), 49−55.
(44) Miller, A. J. M.; Labinger, J. A.; Bercaw, J. E. Trialkylborane-Assisted CO_2 Reduction by Late Transition Metal Hydrides. *Organometallics* **2011**, *30* (16), 4308−4314.
(45) Brereton, K. R.; Smith, N. E.; Hazari, N.; Miller, A. J. M. Thermodynamic and Kinetic Hydricity of Transition Metal Hydrides. *Chem. Soc. Rev.* **2020**, *49* (22), 7929−7948.
(46) Wiedner, E. S.; Chambers, M. B.; Pitman, C. L.; Bullock, R. M.; Miller, A. J. M.; Appel, A. M. Thermodynamic Hydricity of Transition Metal Hydrides. *Chem. Rev.* **2016**, *116* (15), 8655−8692.
(47) Kuett, A.; Leito, I.; Kaljurand, I.; Soovaeli, L.; Vlasov, V. M.; Yagupolskii, L. M.; Koppel, I. A. A Comprehensive Self-Consistent Spectrophotometric Acidity Scale of Neutral Bronsted Acids in Acetonitrile. *J. Org. Chem.* **2006**, *71* (7), 2829−2838.
(48) Kuett, A.; Leito, I.; Kaljurand, I.; Soovaeli, L.; Vlasov, V. M.; Yagupolskii, L. M.; Koppel, I. A. A Comprehensive Self-Consistent Spectrophotometric Acidity Scale of Neutral Bronsted Acids in Acetonitrile. *J. Org. Chem.* **2006**, *71* (7), 2829−2838.
(49) Bullock, R. M.; Bender, B. R. Isotope Methods - Homogeneous. *Encyclopedia of Catalysis*; John Wiley & Sons Ltd.: 2002; p 4.
(50) Svejda, P.; Volman, D. H. Photochemical Formation of Free Radicals from Acetonitrile as Studied by Electron Spin Resonance. *J. Phys. Chem.* **1970**, *74* (9), 1872−1875.
(51) Chandra, H.; Symons, M. C. R. Electron-Addition and Electron-Loss Pathways for Cyanoalkanes. *J. Chem. Soc., Faraday Trans. 1* **1988**, *84* (10), 3401−3412.
(52) Chen, S.; Rousseau, R.; Raugei, S.; Dupuis, M.; DuBois, D. L.; Bullock, R. M. Comprehensive Thermodynamics of Nickel Hydride Bis(Diphosphine) Complexes: A Predictive Model through Computations. *Organometallics* **2011**, *30* (22), 6108−6118.
(53) Warren, J. J.; Tronic, T. A.; Mayer, J. M. Thermochemistry of Proton-Coupled Electron Transfer Reagents and Its Implications. *Chem. Rev.* **2010**, *110* (12), 6961−7001.
(54) Luo, Y.-R. *Comprehensive Handbook of Chemical Bond Energies*; CRC Press: Boca Raton, FL, 2007.
(55) Sang, S.; Unruh, T.; Demeshko, S.; Domenianni, L. I.; Leest, N. P.; Marquetand, P.; Schneck, F.; Würtele, C.; Zwart, F. J.; Bruin, B. Photo-Initiated Cobalt-Catalyzed Radical Olefin Hydrogenation. *Chem. - Eur. J.* **2021**, DOI: 10.1002/chem.202101705.
(56) Hoffman, N. W.; Brown, T. L. Thermal and Photochemical Substitution Reactions of the Tricarbonyl(Cyclopentadienyl)Hydrido Compounds of Tungsten and Molybdenum. *Inorg. Chem.* **1978**, *17* (3), 613−617.
(57) Sweany, R. L. Photolysis of Matrix-Isolated Hydridotetracarbonylcobalt(I). Evidence for Metal-Hydrogen Bond Homolysis. *Inorg. Chem.* **1980**, *19* (11), 3512−3516.
(58) Church, S. P.; Poliakoff, M.; Timney, J. A.; Turner, J. J. The Generation in Solid Carbon Monoxide of the Radical Pentacarbonylmanganese. *J. Mol. Struct.* **1982**, *80*, 159−162.
(59) Sweany, R. L. Photolysis of Matrix-Isolated Hydridotetracarbonylcobalt(I). Comparison of the Probabilities of Carbonyl Loss with Hydrogen Atom Loss. *Inorg. Chem.* **1982**, *21* (2), 752−756.
(60) Bakac, A.; Thomas, L. M.; Espenson, J. H. Macrocyclic Rhodium(III) Hydrides and a Monomeric Rhodium(II) Complex. *Inorg. Chem.* **1996**, *35* (20), 5880−5884.
(61) Yu, M.; Jing, H.; Liu, X.; Fu, X. Visible-Light-Promoted Generation of Hydrogen from the Hydrolysis of Silanes Catalyzed by Rhodium(III) Porphyrins. *Organometallics* **2015**, *34* (24), 5754−5758.
(62) Bandy, J. A.; Cloke, F. G. N.; Copper, G.; Day, J. P.; Girling, R. B.; Graham, R. G.; Green, J. C.; Grinter, R.; Perutz, R. N. Decamethylrhenocene, $(;^5\text{-}C_5Me_5)_2Re$. *J. Am. Chem. Soc.* **1988**, *110* (15), 5039−5050.

https://doi.org/10.1021/jacs.1c10628
J. Am. Chem. Soc. XXXX, XXX, XXX−XXX